Trade-Offs of Chemotactic Foraging in Turbulent Water

John R. Taylor and Roman Stocker

Our results indicate that gene loops act to maintain the directionality of transcription. The loss of a mammalian gene's PAS can directly influence the recruitment of transcription factors, with a consequent reduction in gene expression (22). PAS mutation has also been shown to increase levels of divergent transcripts (23). On the basis of our results, such effects are directly explicable by the loss of gene-loop formation and the potential to recycle factors from the terminator back to the promoter (see model, Fig. 4D). The role of Rpd3S in restricting antisense terminator transcripts (Fig. 3) clearly illustrates the importance of histone deacetylation in preventing inappropriate ncRNA synthesis. We predict that gene loops may similarly act to influence the recruitment of 5′ localized histone deacetylases such as Set3 (24). This would maintain promoters in a deacetylated, inactive state until gene activation selectively promotes transcription of genes rather than divergent pSRTs. We postulate that gene looping contributes to determining which transcription units are fully productive.

References and Notes

1. J. S. Mattick, R. J. Taft, G. J. Faulkner, *Trends Genet.* **26**, 21 (2010).
2. P. Carninci, *Nature* **457**, 974 (2009).
3. L. J. Core, J. T. Lis, *Science* **319**, 1791 (2008).
4. P. Preker et al., *Science* **322**, 1851 (2008).
5. A. C. Seila et al., *Science* **322**, 1849 (2008).
6. H. Neil et al., *Nature* **457**, 1038 (2009).
7. Z. Xu et al., *Nature* **457**, 1033 (2009).
8. J. M. O'Sullivan et al., *Nat. Genet.* **36**, 1014 (2004).
9. A. Ansari, M. Hampsey, *Genes Dev.* **19**, 2969 (2005).
10. B. N. Singh, M. Hampsey, *Mol. Cell* **27**, 806 (2007).
11. S. Medler et al., *J. Biol. Chem.* **286**, 33709 (2011).
12. D. W. Zhang et al., *J. Biol. Chem.* **287**, 8541 (2012).
13. D. L. Pappas Jr., M. Hampsey, *Mol. Cell. Biol.* **20**, 8343 (2000).
14. E. J. Steinmetz, D. A. Brow, *Mol. Cell. Biol.* **23**, 6339 (2003).
15. D. K. Pokholok et al., *Cell* **122**, 517 (2005).
16. L. S. Churchman, J. S. Weissman, *Nature* **469**, 368 (2011).
17. S. C. Murray et al., *Nucleic Acids Res.* **40**, 2432 (2012).
18. M. J. Carrozza et al., *Cell* **123**, 581 (2005).
19. M. C. Keogh et al., *Cell* **123**, 593 (2005).
20. K. J. Perkins, M. Lusic, I. Mitar, M. Giacca, N. J. Proudfoot, *Mol. Cell* **29**, 56 (2008).
21. A. G. Rondón, H. E. Mischo, J. Kawauchi, N. J. Proudfoot, *Mol. Cell* **36**, 88 (2009).
22. C. K. Mapendano, S. Lykke-Andersen, J. Kjems, E. Bertrand, T. H. Jensen, *Mol. Cell* **40**, 410 (2010).
23. P. Preker et al., *Nucleic Acids Res.* **39**, 7179 (2011).
24. T. Kim, S. Buratowski, *Cell* **137**, 259 (2009).
25. T. N. Mavrich et al., *Genome Res.* **18**, 1073 (2008).

Trade-Offs of Chemotactic Foraging in Turbulent Water

John R. Taylor[1] and Roman Stocker[2]*

Bacteria play an indispensable role in marine biogeochemistry by recycling dissolved organic matter. Motile species can exploit small, ephemeral solute patches through chemotaxis and thereby gain a fitness advantage over nonmotile competitors. This competition occurs in a turbulent environment, yet turbulence is generally considered inconsequential for bacterial uptake. In contrast, we show that turbulence affects uptake by stirring nutrient patches into networks of thin filaments that motile bacteria can readily exploit. We find that chemotactic motility is subject to a trade-off between the uptake benefit due to chemotaxis and the cost of locomotion, resulting in an optimal swimming speed. A second trade-off results from the competing effects of stirring and mixing and leads to the prediction that chemotaxis is optimally favored at intermediate turbulence intensities.

The average milliliter of seawater contains a million heterotrophic bacteria that play an essential role in remineralizing dissolved organic matter (DOM) by decomposing 35 to 80% of net primary production (1) and converting it into particulate form, available for consumption by larger organisms. Most marine environments are turbulent, ranging from the energetic mixed-layer and surf zone to calmer thermoclines, yet the effect of turbulence on bacterial uptake of DOM has remained elusive. This is due in part to the difficulty of quantifying the microscale biogeochemical variability generated by turbulence. At the same time, the physics of transport at micrometer scales dictates that DOM uptake occurs primarily by diffusion of nutrient molecules to cells (2). In a homogeneous nutrient environment, marine turbulence is insufficient to increase bacterial uptake (2, 3), at least for low–molecular weight substrates. For example, relatively strong turbulence ($\epsilon = 10^{-6}$ W kg^{-1}, where ϵ is the turbulent dissipation rate) increases the uptake of amino acids by <1%, and as a result turbulence has been considered inconsequential for bacterial uptake (2).

Many DOM sources occur as small, discrete patches, including cell lysis, phytoplankton exudation, marine snow particles, oil droplets, and excretions by larger organisms (4, 5). Numerous bacterial taxa have evolved the ability to sense chemical gradients associated with patches and swim toward more favorable conditions (5–8), a process called chemotaxis. Chemotaxis can affect marine biogeochemical cycles by increasing remineralization rates (5, 9), and community composition by affording motile bacteria a benefit over nonmotile competitors (7). Yet, most knowledge of chemotactic foraging is based on studies in still fluid, simple flows, or synthetic advection (7, 10, 11).

Here, we show that turbulence can affect the relative uptake of DOM by motile and nonmotile bacteria by reshaping the nutrient landscape to which chemotactic bacteria respond. To study the trade-offs of chemotaxis in the turbulent ocean, we used direct numerical simulations (DNS) (12). This method has been applied extensively to model passive scalars in turbulence (13). We use it to resolve the smallest turbulent scales and quantify their impact on the nutrient competition between motile and nonmotile bacteria.

A range of spatial scales affect bacterial foraging in the ocean (Fig. 1). Bacteria experience turbulence as smooth, slowly varying velocity gradients, because their size ($\approx$1 μm) is considerably smaller than the Kolmogorov scale, l_K ($\approx$1 to 10 mm in the ocean) (3), the smallest scale at which turbulent velocity fluctuations occur. Gradients in nutrient concentration persist down to a smaller scale, the Batchelor scale l_B ($\approx$10 to 300 μm in the ocean) (14). Motile bacteria can exploit nutrient gradients if their "motility range"—the distance they can cover over the lifetime of the patch—is larger than the Batchelor scale (Fig. 1). This is generally the case, because bacteria swim up gradients at 5 to 40 μm s^{-1} (8, 15) and can thus travel a distance of l_B in a few seconds.

To determine the impact of turbulence on chemotactic foraging, we used DNS to simulate the competition between motile and nonmotile bacteria for a DOM patch occurring in a turbulent flow (16). The two bacterial species were

[1]Department of Applied Mathematics and Theoretical Physics, University of Cambridge, Wilberforce Road, Cambridge CB3 0WA, UK. [2]Ralph M. Parsons Laboratory, Department of Civil and Environmental Engineering, Massachusetts Institute of Technology, 77 Massachusetts Avenue, Cambridge, MA 02139, USA.

*To whom correspondence should be addressed. E-mail: romans@mit.edu

initially distributed uniformly, each with concentration $B_0 = 2.5 \times 10^{11}$ cells m^{-3}. Bacteria consume nutrients at a rate $1/\tau_U$, where $\tau_U \approx 200$ s is a typical uptake time scale (*16*). Nonmotile bacteria remain uniformly distributed and rely on diffusion to obtain nutrients. Motile bacteria swim up nutrient gradients with a chemotactic velocity that increases with the gradient's magnitude, up to a maximum velocity V_C (*16*). Using dissolved organic carbon as a representative nutrient, we assumed an initial peak concentration of $C_0 = 10 \ \mu M_C$ to reflect the approximately three orders of magnitude concentration enhancement within patches compared to background levels (typical-

ly, 0.1 to 50 nM$_C$) (*17*). In this large difference lies the potential benefit of chemotaxis.

Turbulence affects uptake by reshaping the patch into a complex nutrient landscape (movie S1), dramatically changing the gradients experienced by chemotactic bacteria. Consider motile bacteria ($V_C = 20 \ \mu m \ s^{-1}$) in relatively strong turbulence ($\epsilon = 10^{-6}$ W kg^{-1}) (Fig. 2 and movie S1). Within seconds, turbulence stirs the patch into filaments and sheets as thin as l_B (Fig. 2, top row), which the chemotactic bacteria quickly locate (Fig. 2, bottom row). Fifteen seconds after release of the patch, nutrient filaments are pervasive and harbor concentrations of motile bacte-

ria 50% above background. At 30 s, the patch has morphed into a web of tangled filaments, whose topology is mirrored in the distribution of motile bacteria. After 60 s, the remaining nutrients are well-mixed (the standard deviation of the nutrient concentration is 3.5% of its initial value) and the clustering of motile bacteria begins to fade.

Accumulation of motile bacteria within nutrient-rich filaments increases their uptake rate compared with nonmotile bacteria (Fig. 3A). The difference in the population-averaged, per-cell uptake rate between motile and nonmotile bacteria (*16*) is a measure of the motility benefit. After rescaling

Fig. 1. Physical and biological length scales in the ocean. Turbulent stirring generates variance in the distribution of dissolved nutrients on scales as small as the Batchelor scale, l_B, but does not directly affect the diffusive flux of nutrients on the scales of bacterial cells. However, motile bacteria sample spatial scales considerably larger than their size: Their "motility range" is the distance that they can travel during the lifetime of a typical nutrient patch, while moving up nutrient gradients at the chemotactic velocity V_C. Here, ϵ is the turbulent dissipation rate, ν is the kinematic viscosity of seawater, and κ_C is the nutrient diffusivity.
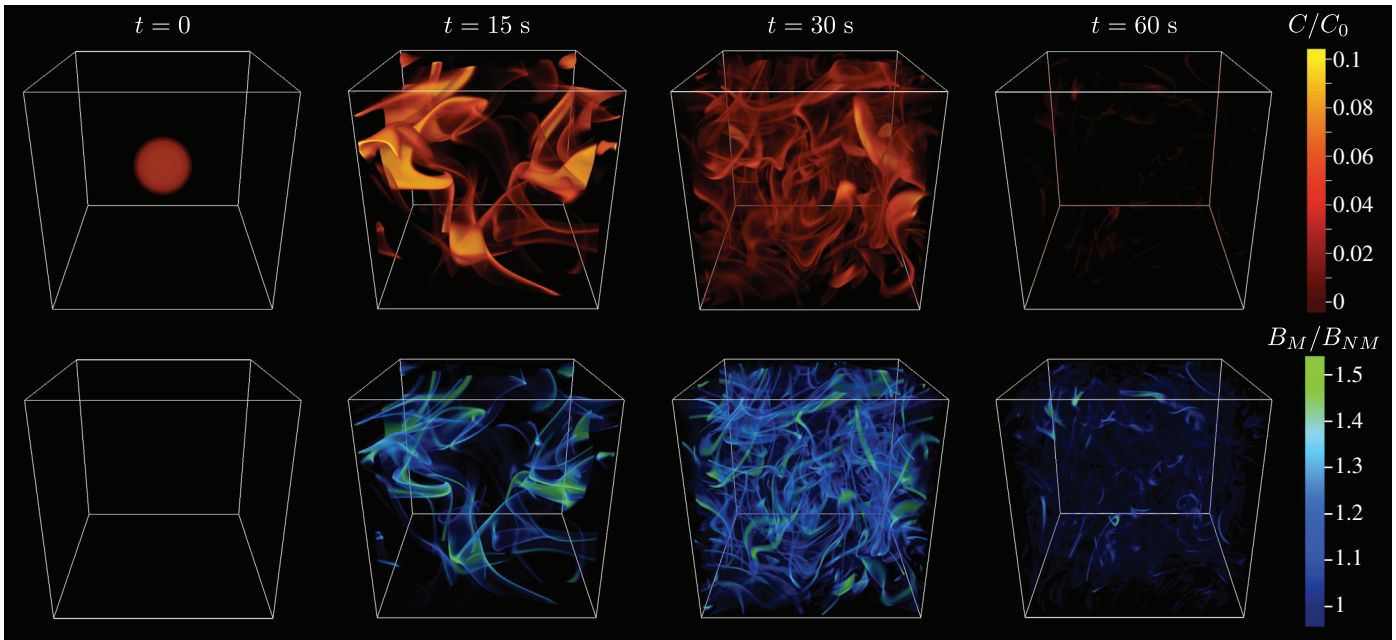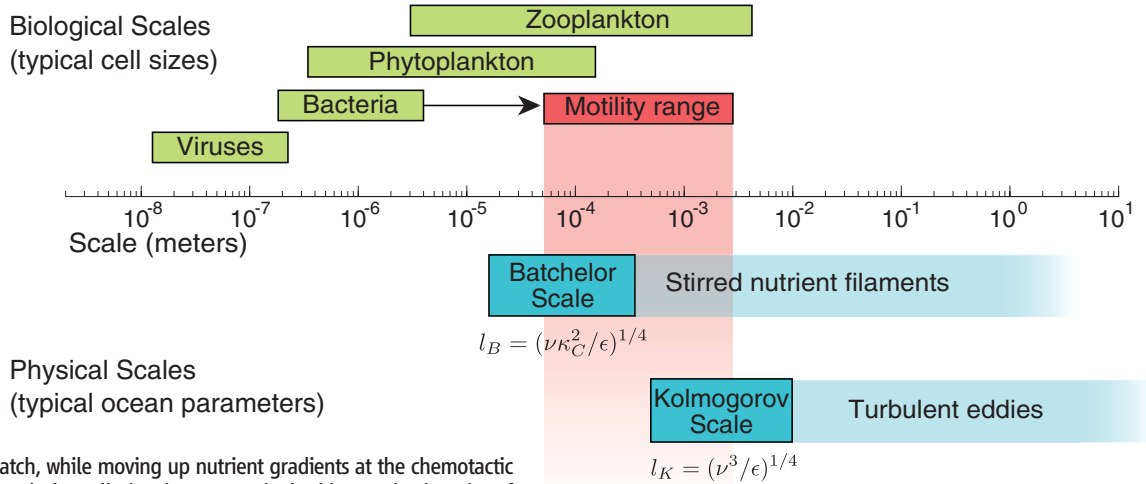
Fig. 2. Stirring of a nutrient patch and response of chemotactic bacteria. As a nutrient patch is stirred by a turbulent flow (top row, showing nutrient concentration C), chemotactic bacteria respond by accumulating within nutrient filaments (bottom row, showing concentration of motile bacteria B_M), thereby enhancing their uptake. For this simulation, the chemotactic velocity was $V_C = 20 \ \mu m \ s^{-1}$, the turbulent dissipation rate $\epsilon = 10^{-6}$ W kg^{-1}, and the domain size $L = 5.65$ cm. Values of C and B_M are normalized by the initial maximum nutrient concentration, C_0, and the concentration of nonmotile bacteria, B_{NM}, respectively. The lowest value on each color scale is made transparent, and opacity increases linearly with concentration. Images generated using Vapor (www.vapor.ucar.edu).

by the number of patches occurring in the computational volume in a day, based on a carbon injection rate of $\dot{C}_{inj} = 0.12$ g_C m^{-3}day^{-1} (16), and by the carbon content in one cell (16), the motility benefit can be expressed in units of new cell equivalents produced by each bacterium per day. For the scenario shown in Fig. 2, the motility benefit peaks 13.2 s after injection of the patch. At this time, motile cells consume 23% more than nonmotile cells, an equivalent benefit of more than one new cell per day (per individual) if the uptake difference was sustained at this level (relative to 4.5 new cells per day produced by each cell of either species in the absence of chemotaxis). Instead, the motility benefit nearly vanishes after 50 s, even though 59% of the nutrient is still available, because what remains has been mixed, erasing any advantage of motility.

The instantaneous motility benefit, like the nutrient filaments, is therefore highly transient.

To determine the chemotactic velocity that optimizes foraging, we performed competition simulations where we varied the maximum chemotactic velocity, V_C, while keeping the turbulence intensity constant at an intermediate level ($\epsilon = 1.2 \times 10^{-8}$ W kg^{-1}). The advantage afforded by chemotaxis depends strongly on V_C (Fig. 3, A and B). The motility benefit is weak throughout the patch lifetime for slow chemotaxers. For example, motility enhances the instantaneous uptake by at most 15%, affording a time-averaged benefit of 0.3 new cells per day, for $V_C = 5$ μm s^{-1}. A chemotactic velocity of this order is typical of the enteric bacterium *Escherichia coli* ($V_C = 0.6$ to 13.8 μm s^{-1}) (15), the traditional model organism for the study of chemotaxis. In contrast,

marine bacteria are capable of much higher swimming speeds (up to a few hundred μm s^{-1}) and high-performance chemotaxis (6, 7, 18). For chemotactic velocities of $V_C = 20$ to 60 μm s^{-1}, associated with swimming speeds of $V_S = 60$ to 170 μm s^{-1} (16), the motility benefit can be much larger, with motile cells instantaneously consuming up to 58 to 133% more than nonmotile cells and experiencing a time-averaged benefit of 1.1 to 2.3 additional new cells per day (Fig. 3, A and B).

Motility can be costly for marine bacteria. The motility benefit grows approximately linearly with chemotactic velocity (Fig. 3B), whereas propulsive power increases quadratically with the swimming speed (16). This suggests a trade-off between enhanced uptake and swimming cost, and the existence of an optimal chemotactic velocity. To test this prediction, we computed the
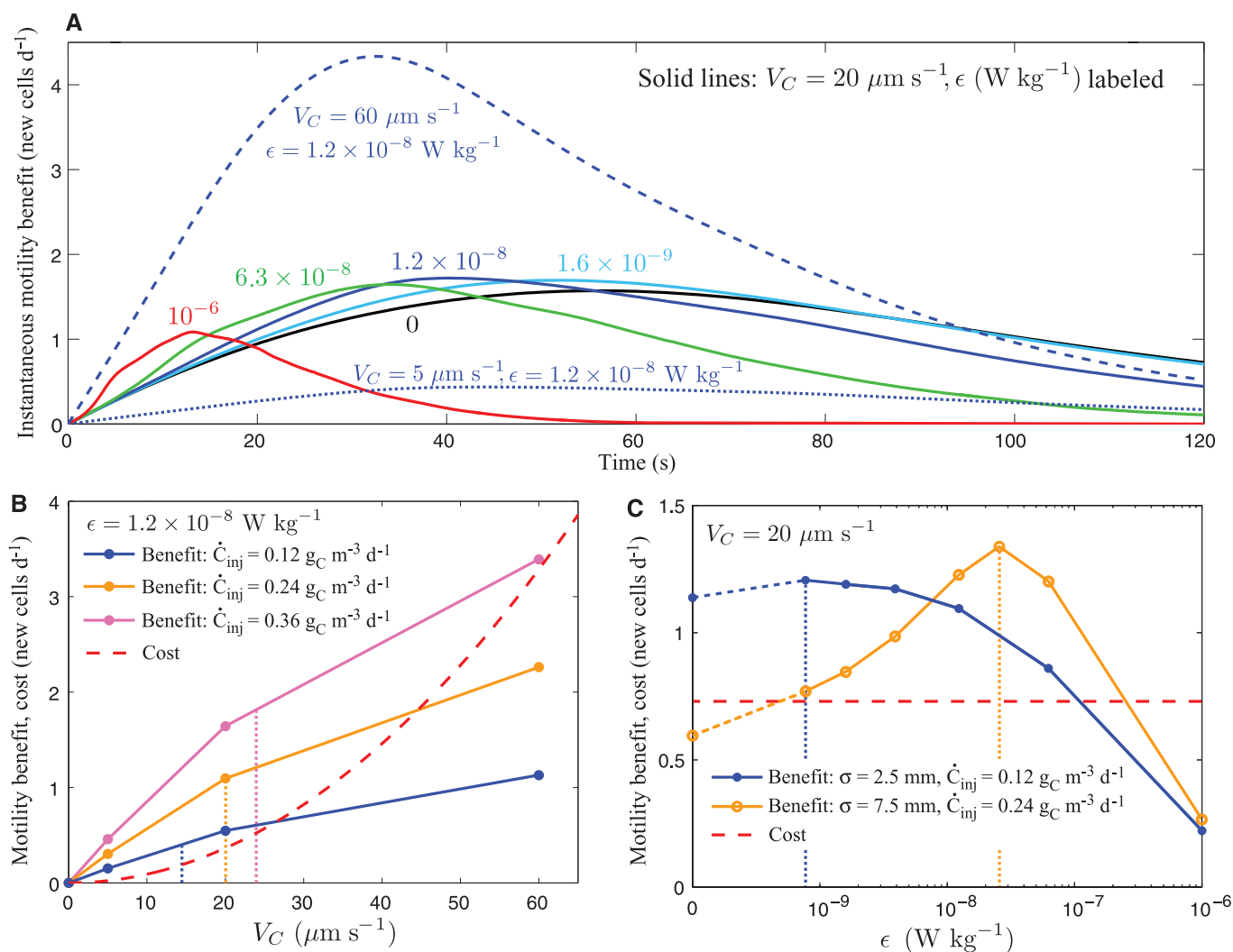
Fig. 3. Trade-offs of chemotactic foraging. (**A**) The instantaneous motility benefit as a function of time since release of the nutrient patch, for different turbulence intensities ε and chemotactic velocities V_C. (**B**) The motility benefit, shown for three carbon injection rates $\dot{C}_{inj}$ (solid lines), increases with the chemotactic velocity V_C, but the cost of swimming (dashed red line) increases more rapidly (quadratically) with V_C. The trade-off between motility benefit and swimming cost results in an optimal chemotactic velocity (dotted lines) of $V_C \approx 15$ to 25 μm s^{-1}. (**C**) The trade-off between stirring and mixing results in an optimal value of turbulence (dotted lines) that depends on the initial patch size, σ. For large patches, the motility benefit is optimal in moderate turbulence (orange line), whereas smaller patches lead to an optimum in weak turbulence (blue line). Values of the motility benefit in the absence of flow (ε = 0) are connected with dashed lines (values of ε < 7.7 × 10^{-10} W kg^{-1} were not considered owing to computational restrictions).

net motility benefit as the difference between the motility benefit and the power required for swimming [16]. In intermediate turbulence ($\epsilon = 1.2 \times 10^{-8}$ W kg^{-1}), the net motility benefit is maximal for $V_C \approx 15$ to 25 μm s^{-1} (Fig. 3B), corresponding to swimming speeds V_S of 45 to 70 μm s^{-1} [16]. These values are in good agreement with speeds recorded for several species of marine bacteria [6–8, 18, 19], suggesting that motility in marine bacteria might be under selection for chemotactic fitness.

The effectiveness of chemotaxis as a foraging strategy further depends on the intensity of turbulence through the stirring and mixing of nutrient patches. We quantified this dependence by varying the turbulence intensity, while keeping the chemotactic velocity constant ($V_C = 20$ μm s^{-1}). For an initial patch size of σ = 2.5 mm, chemotaxis is optimally favored at weak turbulence intensities ($\epsilon \approx 10^{-9}$ W kg^{-1}), characteristic of the ocean thermocline [20], where the motility benefit is slightly larger than in the absence of turbulence (Fig. 3C). In contrast, the motility benefit is fivefold smaller at $\epsilon = 10^{-6}$ W kg^{-1} (Fig. 3C), indicating that chemotaxis is less effective in highly turbulent regions, such as the upper ocean. For larger patches the optimum turbulence intensity shifts to intermediate values ($\epsilon \approx 10^{-8}$ to 10^{-7} W kg^{-1} for σ = 7.5 mm; Fig. 3C), characteristic of the upper thermocline [20]. Although observations of motility in the ocean are insufficient to test these predictions, it will be interesting to determine whether changes in the prevalence of motility and chemotaxis with depth revealed by metagenomic studies [21] are in part determined by turbulence levels.

The existence of an optimal turbulence intensity points to a second, more subtle trade-off: that between stirring and mixing. Stirring increases the surface area between the nutrient patch and the surrounding water (Fig. 2). Mixing refers to homogenization of the nutrients, which is aided by stirring but ultimately occurs by molecular diffusion. Stronger turbulence produces thinner filaments and steeper nutrient gradients that elicit faster chemotaxis, but also accelerates mixing, which erases the motility benefit. This trade-off results in an optimal turbulence intensity, whereby the maximum motility benefit depends jointly on the size and lifetime of DOM filaments.

Constraints on chemotaxis can be understood in terms of three fundamental time scales [16]. The chemotaxis time scale, $\tau_C = l_B/V_C$, is the time it takes a bacterium to swim to the core of a nutrient filament, whose characteristic width is the Batchelor scale, l_B. Stronger turbulence creates finer filaments (smaller l_B and τ_C), but also decreases the filaments' lifetime, which is characterized by the mixing time scale, $\tau_M = l_B^2/\kappa_C$, where κ_C is the nutrient diffusivity. One thus expects that the motility benefit depends on the relative magnitude of τ_C and τ_M. A further condition for motility to be beneficial is that the consumption of the patch through uptake is slower

than chemotactic migration, i.e., $\tau_C < \tau_U$. We quantify the relative magnitude of the three time scales by means of two Frost numbers, $Fr_M = \tau_C/\tau_M$ and $Fr_U = \tau_C/\tau_U$ [16, 22]. When $Fr_M \gg 1$ or $Fr_U \gg 1$, chemotaxis is too slow relative to mixing (the "mixing-limited regime") or consumption (the "uptake-limited regime"), respectively, for motile bacteria to gain appreciable benefit. This argument is verified by a formal scaling analysis [16], whose prediction (Eq. S40) is in good agreement with the DNS results.

In addition to swimming speed and turbulence intensity, the net benefit of chemotaxis depends on multiple features of the nutrient landscape, as additional simulations reveal [16]. The total nutrient injection rate must be sufficient to justify the investment in motility. We used a baseline value of 0.12 g_C m^{-3} day^{-1}, representative of relatively nutrient-rich conditions [1, 16]. Fast chemotaxis is optimal at higher injection rates (Fig. 3B), whereas lower input rates shift the competition in favor of nonmotile bacteria, in line with evidence that abundant species in the oligotrophic open ocean are nonmotile [23]. The benefit of chemotaxis further depends on patch size. In the absence of flow, the motility benefit is optimal for a patch size of σ ≈ 650 μm; larger patches are too vast for bacteria to reach their nutrient-rich core, whereas smaller patches quickly diffuse away. The motility benefit is less dependent on the initial patch size in a turbulent flow, because the patch is stirred into Batchelor-scale filaments. Therefore, turbulence can significantly favor the utilization of larger patches by motile bacteria (Fig. 3C). Finally, an important role is played by the nutrient diffusivity, because higher–molecular weight solutes, abundant in the ocean, diffuse more slowly, prolonging the filaments' lifetime and favoring chemotaxis [16]. Taken together, these findings indicate that, although our fundamental conclusions apply to a broad range of nutrient conditions, the net motility benefit is environment-dependent: It will be lower than predicted here, or vanish entirely, for oligotrophic conditions or very small patches, and it might be higher for intermediate patch sizes or high–molecular weight solutes.

Our results indicate that, in contrast to *E. coli* [24], motile marine bacteria spend a sizable fraction of their metabolic budget on locomotion. Whereas many coastal ocean bacteria are motile [9, 25], dominant clades in the open ocean, like SAR11 [23], are nonmotile, providing evidence that motility is not without cost. We propose that a fundamental determinant of the prevalence of motility in a given environment is the trade-off between motility benefit and swimming cost. Chemotaxis in the heterogeneous, time-varying nutrient landscape prevalent in the ocean should be seen as an optimal foraging problem, where the most successful strategy depends on the nutrient distribution and turbulence intensity. In addition to the trade-offs presented here, other factors can affect the optimal foraging behavior. Additional costs, associated with biosynthesis of flagel-

la, operation of chemotaxis pathways, increased encounter rates with predators, and less effective uptake kinetics, might reduce the optimal chemotactic velocity and the net motility benefit. In contrast, the benefits of motility could be augmented by the ability of fast cells to escape capture [26] or to modulate swimming so as to combine intermediate exploration speeds with fast exploitation speeds [27]. Indeed, most bacteria remain outside of nutrient filaments (e.g., less than 1.7% of the cells experience $C > 0.01 C_0$ at any given time) and can be considered in "exploration mode," using undirected motility to search for a chemical signal that they can exploit through chemotaxis.

DNS provides a quantitative framework to investigate this optimal foraging problem, and we have applied it to show that turbulence can affect the competition between motile and nonmotile bacteria. The outcome of this competition will be an important determinant of species succession when environmental conditions change—for example, during algal blooms or oil spills, when the abundance of DOM sources varies greatly. More broadly, DNS promises to be a valuable tool to address the elusive effects of turbulence on microscale biophysical processes, such as gamete encounter rates [28], phytoplankton patchiness [29], microbial productivity in bioreactors [30], and the fate of microbial nutrient sources, including particle plumes and oil droplets.

The results presented here upend the prevailing view on the effect of turbulence on aquatic microorganisms. Contrary to current understanding, based on homogeneous nutrient environments where turbulence is inconsequential for bacterial uptake [2], motile bacteria are directly affected by fluid motion in a heterogeneous environment, where they can exploit thin nutrient filaments generated by turbulence. This process generalizes to a broad spectrum of nutrient sources, because turbulence will stir even large DOM patches into a tangled web of filaments. Accordingly, the nutrient landscape experienced by aquatic microorganisms might be even more heterogeneous and intermittent than previously thought [4], renewing the challenge of capturing the effect of this variability on microbial adaptations and marine biochemistry.

References and Notes
1. C. Duarte, J. Cebrian, *Limnol. Oceanogr.* **41**, 1758 (1996).
2. L. Karp-Boss, E. Boss, P. Jumars, *Oceanogr. Mar. Biol. Annu. Rev.* **34**, 71 (1996).
3. J. Lazier, K. Mann, *Deep Sea Res. A* **36**, 1721 (1989).
4. F. Azam, F. Malfatti, *Nat. Rev. Microbiol.* **5**, 782 (2007).
5. N. Blackburn, T. Fenchel, J. Mitchell, *Science* **282**, 2254 (1998).
6. J. G. Mitchell, L. Pearson, S. Dillon, *Appl. Environ. Microbiol.* **62**, 3716 (1996).
7. R. Stocker, J. R. Seymour, A. Samadani, D. E. Hunt, M. F. Polz, *Proc. Natl. Acad. Sci. U.S.A.* **105**, 4209 (2008).
8. J. R. Seymour, R. Simó, T. Ahmed, R. Stocker, *Science* **329**, 342 (2010).
9. T. Fenchel, *Science* **296**, 1068 (2002).

10. T. Kiørboe, G. Jackson, *Limnol. Oceanogr.* **46**, 1309 (2001).
11. J. Muñoz-García, Z. Neufeld, C. Torney, *New J. Phys.* **12**, 103043 (2010).
12. P. Moin, K. Mahesh, *Annu. Rev. Fluid Mech.* **30**, 539 (1998).
13. D. Donzis, K. Sreenivasan, P. Yeung, *Flow Turbul. Combus.* **85**, 549 (2010).
14. G. Batchelor, *J. Fluid Mech.* **5**, 113 (1959).
15. T. Ahmed, R. Stocker, *Biophys. J.* **95**, 4481 (2008).
16. Supplementary materials are available on *Science* Online.
17. P. Williams, in *Microbial Ecology of the Oceans*, D. L. Kirchman, Ed. (Wiley, New York, 2000), pp. 153–200.
18. L. Xie, T. Altindal, S. Chattopadhyay, X. L. Wu, *Proc. Natl. Acad. Sci. U.S.A.* **108**, 2246 (2011).
19. A. Hütz, K. Schubert, J. Overmann, *Appl. Environ. Microbiol.* **77**, 4412 (2011).
20. M. Gregg, D. Winkel, T. Sanford, H. Peters, *Dyn. Atmos. Oceans* **24**, 1 (1996).
21. E. F. DeLong *et al.*, *Science* **311**, 496 (2006).
22. D. Grünbaum, *Hydrobiologia* **480**, 175 (2002).
23. R. M. Morris *et al.*, *Nature* **420**, 806 (2002).
24. E. Purcell, *Am. J. Phys.* **45**, 3 (1977).
25. H. Grossart, L. Riemann, F. Azam, *Aquat. Microb. Ecol.* **25**, 247 (2001).
26. C. Matz, K. Jürgens, *Appl. Environ. Microbiol.* **71**, 921 (2005).
27. J. Seymour, Marcos, R. Stocker, *Am. Nat.* **173**, E15 (2009).
28. J. Crimaldi, H. Browning, *J. Mar. Syst.* **49**, 3 (2004).
29. W. M. Durham, E. Climent, R. Stocker, *Phys. Rev. Lett.* **106**, 238102 (2011).
30. J. Marshall, Y. Huang, *Chem. Eng. Sci.* **65**, 3865 (2010).

Asymmetric Division of *Drosophila* Male Germline Stem Cell Shows Asymmetric Histone Distribution

Vuong Tran,* Cindy Lim,* Jing Xie, Xin Chen†

Stem cells can self-renew and generate differentiating daughter cells. It is not known whether these cells maintain their epigenetic information during asymmetric division. Using a dual-color method to differentially label "old" versus "new" histones in *Drosophila* male germline stem cells (GSCs), we show that preexisting canonical H3, but not variant H3.3, histones are selectively segregated to the GSC, whereas newly synthesized histones incorporated during DNA replication are enriched in the differentiating daughter cell. The asymmetric histone distribution occurs in GSCs but not in symmetrically dividing progenitor cells. Furthermore, if GSCs are genetically manipulated to divide symmetrically, this asymmetric mode is lost. This work suggests that stem cells retain preexisting canonical histones during asymmetric cell divisions, probably as a mechanism to maintain their unique molecular properties.

Although all cells in an organism contain the same genetic material, different genes are expressed in specific cell types, allowing them to differentiate along distinct pathways. Epigenetic mechanisms regulate gene expression and maintain a specific cell fate through many cell divisions (*1*–*3*). Stem cells have the remarkable ability to both self-renew and generate daughter cells that enter differentiation (*4*). Epigenetic mechanisms have been reported to regulate stem cell activity in multiple lineages (*5*–*7*). However, there has been little direct in vivo evidence demonstrating whether stem cells retain their epigenetic information.

The *Drosophila* male GSCs are well characterized in terms of their physiological location, microenvironment (i.e., niche), and cellular structures (*8*, *9*) (Fig. 1, A and B). Male GSCs can be identified precisely by their distinct anatomical positions and morphological features. A GSC usually divides asymmetrically to produce a self-renewed GSC and a daughter cell gonialblast (GB) that undergoes differentiation. Therefore, GSCs can be examined at single-cell resolution for a direct comparison.

In eukaryotes, the basic unit of chromatin called nucleosome contains histone octamer [2×(H3, H4, H2A, H2B)] and DNA wrapping around them. Indeed, histones are one of the major carriers of epigenetic information (*10*). To address how histones are distributed during the GSC asymmetric division, we developed a switchable dual-color method to differentially label "old" versus "new" histones (Fig. 1C) that uses both spatial (by Gal4; UAS system) and temporal (by heat shock induction) controls to switch labeled histones from green [green fluorescent protein (GFP)] to red [monomeric Kusabira-Orange (mKO)]. Heat shock treatment induces an irreversible DNA recombination to shut down expression of GFP-labeled old histones and initiate expression of mKO-labeled new histones. If the old histones are partitioned nonselectively, the GFP will initially exhibit equal distribution in the GSC and GB, and will be gradually replaced by the mKO (Fig. 1D). However, if the old histones are preferentially retained in the GSCs to constitute potentially GSC-specific chromatin structure, the GFP will be detected specifically in the GSCs (Fig. 1E). During DNA replication–dependent canonical histone deposition, histones H3 and H4 are incorporated as a tetramer, and histones H2A and H2B are incorporated as dimers (*11*–*15*). Therefore, we generated independent transgenic strains for H3 and H2B, respectively. On the other hand, histone variants are incorporated into chromatin in a transcription-coupled but DNA replication–independent manner (*16*, *17*). Therefore, the histone variant H3.3 was used as a control for canonical histones.

To avoid potential complications caused by heat shock–induced DNA recombination on either one or both chromosomes in GSCs, each of the three transgenes (H3, H2B, and H3.3) was integrated as a single copy and analyzed in heterozygous flies. Examination of testes with the transgenes revealed nuclear GFP but little mKO signal before heat shock. After heat shock, mKO signals were detectable (fig. S1). Different GSCs undergo mitosis asynchronously, and an average cell cycle length of GSCs is approximately 12 to 16 hours. Among all GSCs, 75 to 77% are in G_2 phase, 21% are in S phase, fewer than 2% are in mitosis, and G_1-phase GSCs are almost negligible (*18*–*22*). Moreover, the GSC and GB arising from an asymmetric division remain connected after mitosis by a cellular structure known as the spectrosome, when they undergo the next G_1 and S phases synchronously (*19*, *21*).

To examine the distribution of old versus new histones in GSC and GB after a round of DNA replication–dependent histone deposition, we studied testes 16 to 20 hours after heat shock (Fig. 2A). In particular, GSC-GB pairs connected by spectrosomes were examined (Fig. 2, B and H, arrows). On the basis of cell cycle length of GSCs, these GSC-GB pairs were from GSCs that switched from *histone-GFP* to *histone-mKO* genetic code during their G_2 phase and then underwent the first mitosis followed by G_1, S, and G_2 phase and the second mitosis (Fig. 2A). Within this time frame, both old histones

Department of Biology, Johns Hopkins University, Baltimore, MD 21218, USA.

*These authors contributed equally to this work.
†To whom correspondence should be addressed. E-mail: xchen32@jhu.edu